Discovery of Elgoresyite, (Mg,Fe)5Si2O9: Implications for Novel Iron Magnesium Silicates in Rocky Planetary Interiors

Luca Bindi, Ryosuke Sinmyo, Elena Bykova, Sergey, V Ovsyannikov, Catherine Mccammon, Ilya Kupenko, Leyla Ismailova, Leonid Dubrovinsky, Xiande Xie

ACS EARTH AND SPACE CHEMISTRY

http://pubs.acs.org/journal/aesccq

Article

Discovery of Elgoresyite, $(Mg,Fe)_5Si_2O_9$: Implications for Novel Iron-Magnesium Silicates in Rocky Planetary Interiors

Luca Bindi,* Ryosuke Sinmyo, Elena Bykova, Sergey V. Ovsyannikov, Catherine McCammon, Ilya Kupenko, Leyla Ismailova, Leonid Dubrovinsky, and Xiande Xie

Cite This: *ACS Earth Space Chem.* 2021, 5, 2124–2130

Read Online

ACCESS | Metrics & More | Article Recommendations | Supporting Information

ABSTRACT: As the most abundant material of rocky planets, high-pressure polymorphs of iron- and aluminum-bearing magnesium silicates have long been sought by both observations and experiments. Meanwhile, it was recently revealed that iron oxides form $(FeO)_m(Fe_2O_3)_n$ homologous series above ~10 GPa according to laboratory high-pressure experiments. Here, we report a new high-pressure iron-magnesium silicate, recently approved by the International Mineralogical Association as a new mineral (No. 2020-086) and named elgoresyite, in a shock-induced melt vein of the Suizhou L6 chondrite with a chemistry of $(Mg,Fe)_5Si_2O_9$. The crystal structure of this new silicate is the same as the iron oxide Fe_7O_9, strongly suggesting that silicates also form $((Mg,Fe)O)_{m+n}(SiO_2)_n$ series that are isostructural to iron oxides via $(Mg^{2+},Fe^{2+}) + Si^{4+} = 2Fe^{3+}$ substitution. To test this hypothesis, the phase relationships of the silicates and iron oxides should be further investigated at higher temperature conditions. Newly found iron-magnesium silicate is a potential constituent mineral in rocky planets with relatively high MgO + FeO content.

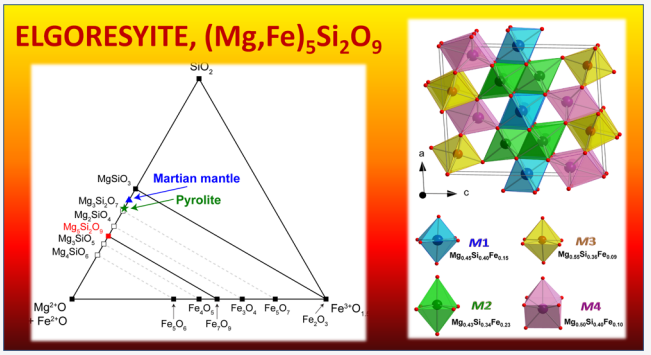

KEYWORDS: *interior of the Earth and planets, iron oxide, silicate, high-pressure and high-temperature, meteorite*

INTRODUCTION

According to the current state-of-the-art knowledge, more than half of the Earth by volume is made of iron- and aluminum-bearing magnesium silicates. As the dominant constituent materials, the stability of these compounds is fundamental to understanding the structure and dynamics of Earth and rocky planets, such as Mercury, Venus, and Mars. The seismic discontinuities observed in Earth's deep mantle can be explained by phase transitions and chemical transformations of the magnesium silicates to denser form.[1−4] Changes in phase and chemical composition are expected to have a strong effect on mantle convection and the thermal history of Earth.[5,6] The types of mantle convection are likely different between rocky planets, partly because of variations in their bulk chemistry and resultant constituent magnesium-rich silicates. For instance, the most abundant mineral in Earth, $MgSiO_3$-rich bridgmanite,[7] may not be stable in the Martian mantle because of the low internal pressure. It is suggested that the types of convection largely vary depending on the absence or presence of a bridgmanite layer inside Mars.[8] This may lead to different thermal histories between Earth and Mars. Likewise, the chemical evolution of the rocky planets has been strongly controlled by the melting phase relationships of magnesium silicate.[9−11] Freezing of Earth's magma ocean has possibly generated rocks enriched in bridgmanite, which can be a geochemical reservoir of different elements due to its high viscosity.[12]

Although planetary interiors are mostly under high-pressure conditions, high-pressure polymorphs of magnesium silicates have been rarely found in natural rock samples due to retrograde reactions to low-pressure phases during their ascent to the surface.[13,14] Instead, the stability of iron-bearing magnesium silicates has long been understood based on experiments, seismology, and observations of shocked meteorites. According to laboratory high-pressure experiments, $(Mg,Fe)_2SiO_4$ olivine undergoes a phase transition to wadsleyite and ringwoodite at ~14 and ~18 GPa, respectively.[4] The crystal structure of ringwoodite is a spinel-type with four- and sixfold coordinated cation sites for Si^{4+} and M^{2+} ($M^{2+} = Mg^{2+} + Fe^{2+}$), respectively. Ringwoodite breaks down to $(Mg,Fe)SiO_3$ bridgmanite and $(Mg,Fe)O$ ferropericlase at ~24 GPa.[1,2] Bridgmanite has six- and eightfold cation sites for SiO_6 and MO_8. It is known that bridgmanite further transforms

Received: May 24, 2021
Revised: July 13, 2021
Accepted: July 14, 2021
Published: July 22, 2021

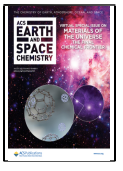

into post-perovskite at ~120 GPa.[3] Seismic discontinuities observed at 410 and 660 km depths are commonly accepted to be related to phase transitions from olivine to wadsleyite and from ringwoodite to bridgmanite + ferropericlase, respectively. The high-pressure polymorphs are consequently found in naturally occurring shock-induced melt veins of meteorites, such as ringwoodite,[15] bridgmanite,[7] and hiroseite.[16] Minerals trapped in diamonds are claimed to have been delivered from the deep mantle based on the bulk chemistry of their inclusions.[17,18] However, recognizing them as high-pressure phases is difficult as their original crystal structures are rarely preserved. Indeed, only four X-ray diffraction spots from a high-pressure magnesium silicate crystal (ringwoodite) have ever been observed from a diamond inclusion.[14] Recently, many iron oxide phases have been discovered experimentally in the Fe−O system at high-pressure conditions above 5−10 GPa with novel crystal structures and stoichiometries.[19−23] Iron oxides form a $(FeO)_m(Fe_2O_3)_n$ homologous series[24] that includes, for example, Fe_4O_5 (m = 2, n = 1), Fe_5O_6 (m = 3, n = 1), Fe_5O_7 (m = 1, n = 2), and Fe_7O_9 (m = 3, n = 2). The homologous series is based on crystallographic building blocks of two types of FeO_6 polyhedra: octahedra and prisms.[23] Possible relics of these new high-pressure phases have been reported in diamond inclusions with various redox conditions.[24,25]

Here, we report a new naturally occurring high-pressure iron-magnesium silicate in a shock-induced melt vein of the Suizhou meteorite with $(Mg,Fe)_5Si_2O_9$ model stoichiometry. It has been accepted as a new mineral by the Commission on New Minerals and Nomenclature Classification of the International Mineralogical Association (No. 2020-086) and named elgoresyite after Ahmed El Goresy, a highly regarded mineralogist working on planetary materials. The holotype material containing elgoresyite is deposited in the collections of the Museo di Storia Naturale, Università degli Studi di Firenze, Firenze, Italy, catalogue number 3238/I.

Elgoresyite exhibits the same crystal structure as the high-pressure iron oxide Fe_7O_9 stable at 24−26 GPa and 1873−1973 K.[22] This new iron-magnesium silicate may be a constituent mineral of iron-rich rocky planetary interiors that have relatively high $MgO/(MgO + SiO_2)$ ratios. Additionally, this finding strongly suggests that iron-bearing magnesium silicates could adopt crystal structures in a homologous series analogous to high-pressure iron oxides. Moreover, as a potential liquidus phase of deep magmas, new iron-magnesium silicates would control the chemical evolution of rocky planetary interiors.

METHODS AND RESULTS

Occurrence. Elgoresyite was detected as a unique grain in a shock-induced melt vein of the Suizhou meteorite. Suizhou L6 chondrite is a shocked meteorite with the occurrence of thin shock-induced melt veins less than 300 μm in thickness. The shock-induced melt veins contain abundant high-pressure polymorphs including ringwoodite, majorite, majorite-pyrope garnet, akimotoite, magnesiowüstite, lingunite, tuite, xieite, a tetragonal form of ringwoodite, hemleyite, asimowite, and hiroseite.[16,26−36] During a crystallographic study of the different high-pressure phases present in the shock-induced melt veins of the Suizhou meteorite, several ringwoodite grains were investigated by single-crystal X-ray diffraction. During this search, most of the grains turned out to be ringwoodite with the canonical cubic *Fd*-3*m* spinel structure. However, one of them (indicated as SPD in Figure 1) turned out to be a tetragonal variant of ringwoodite and it was described in detail

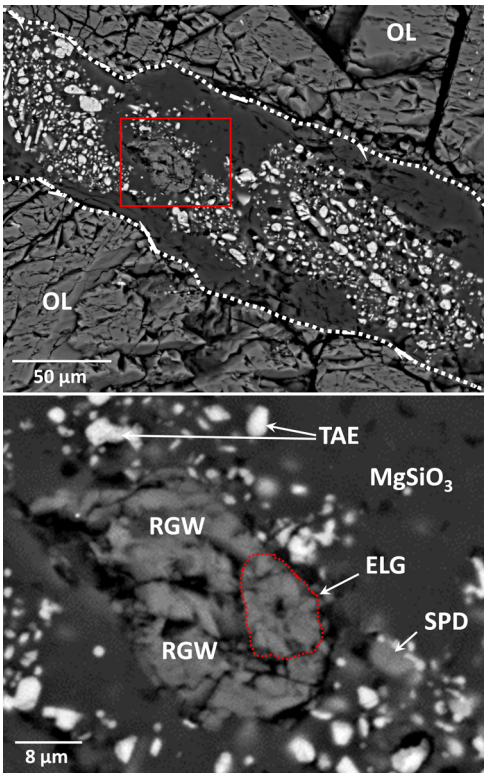

Figure 1. Scanning electron microscopy image of the newly found iron-magnesium silicate. Top: SEM-BSE panoramic image of the section containing new magnesium silicate (OL: olivine). The dashed lines indicate the walls of the shock-induced melt vein. The red rectangular area indicates the region enlarged in the bottom BSE image. Bottom: enlarged area depicted in the top panel; elgoresyite (ELG) [$(Mg,Fe)_5Si_2O_9$], indicated with the dotted red line, is associated with ringwoodite (RGW), olivine (OL), tetragonal ringwoodite (SPD), taenite (TAE), and $MgSiO_3$-rich glass.

by Bindi et al.[27] Furthermore, when the ringwoodite grain (indicated as RGW in the bottom panel of Figure 1) was checked, it was found to be composed of two phases with almost identical chemical composition: one is ringwoodite and the other turned out to be elgoresyite (indicated as ELG in Figure 1). The two phases are almost indistinguishable in the SEM-back-scattered electron image shown in Figure 1 as they are almost identical from the chemical point of view. Indeed, if the chemical data of elgoresyite are normalized on the basis of four oxygen atoms, we obtain $(Mg_{1.48}Fe_{0.70})_{\Sigma = 2.18}Si_{0.85}O_4$, which is close to the Suizhou ringwoodite stoichiometry, i.e., $(Mg_{1.58}Fe_{0.42})SiO_4$. This could imply that elgoresyite could be much more common than thought in shock-induced melt veins of meteorites due to misidentification as ringwoodite.

Appearance and Properties. Elgoresyite occurs as a very rare, subhedral μm-sized crystal closely associated with ringwoodite in a $MgSiO_3$ glass (Figure 1). The fragment used for the X-ray investigation (dotted red line in the bottom panel of Figure 1), is about 6 × 8 × 10 μm^3 in size. Color, luster, streak, hardness, tenacity, cleavage, fracture, and density could not be determined because of the small grain size, and optical properties could also not be determined because of the small grain size. The mean refractive index ($n = K_c * D + 1$) is

https://doi.org/10.1021/acsearthspacechem.1c00157
ACS Earth Space Chem. 2021, 5, 2124−2130

1.95 on the basis of the Gladstone–Dale relationship. Density (calc) is 4.315 g·cm^{-3} based on the empirical formula and single-crystal XRD data.

Chemical Data. A preliminary chemical analysis using EDS performed on the crystal fragment used for the structural study did not indicate the presence of elements ($Z > 9$) other than Mg, Fe, Si, and minor Na, Al, and Ca. Analyses (4) were then carried out using a JEOL 8200 microprobe (WDS mode, 15 kV, 10 nA, 1 μm beam size, counting times 20 s for peak and 10 s for background). For the WDS analyses the $K\alpha$ lines for all the elements were used. The crystal fragment was found to be homogeneous within analytical error. Analytical data are given in Supporting Information Table ST1. The empirical formula (based on nine oxygen atoms *pfu*) is $(Mg_{3.38}Si_{1.95}Fe^{2+}_{1.60}Al_{0.05}Na_{0.03}Ca_{0.02})_{\Sigma = 7.03}O_9$. The simplified and ideal chemical formula is $(Mg,Fe,Si)_7O_9$.

Crystallography. Single-crystal X-ray studies were carried out using a Bruker D8 Venture diffractometer equipped with a Photon II CCD detector, with graphite-monochromatized Mo$K\alpha$ radiation (λ = 0.71073 Å), with 30 s exposure time per frame; the detector-to-sample distance was 6 cm. The crystal system is monoclinic, and the space group is $C2/m$ (#12). The unit cell parameters are: a = 9.397(2) Å, b = 2.763(1) Å, c = 11.088(3) Å, β = 94.25(2)°, V =287.10(14) Å^3, and Z = 2. X-ray powder diffraction data (Supporting Information Table ST2) were obtained with a Bruker D8 Venture diffractometer equipped with a Photon III CCD detector and using copper radiation (CuKα, λ = 1.54138 Å) with 600 s of exposure; the detector-to-sample distance was 7 cm. The program APEX3[37] was used to convert the observed diffraction rings to a conventional powder diffraction pattern. The least-squares refinement gave the following values; crystal system: monoclinic, space group: $C2/m$ (#12), a = 9.3946(4) Å, b = 2.7640(1) Å, c = 11.0804(5) Å, β = 94.233(4)°, V = 286.94(1) Å^3, and Z = 2.

Crystal Structure. The small elgoresyite fragment was extracted from the polished section under a reflected light microscope and mounted on a 5 μm diameter carbon fiber, which was, in turn, attached to a glass rod. Single-crystal X-ray diffraction intensity data of the sample were integrated and corrected for standard Lorentz polarization factors and absorption with the APEX3 software.[37] A total of 732 unique reflections were collected. Given the similarity in the unit cell values and in the space groups, the structure was refined starting from the atomic coordinates reported for synthetic Fe_7O_9[22] using the program SHELXL-97.[38] The site occupation factor (s.o.f.) at the cation sites was allowed to vary (Fe vs Mg for the M sites) using scattering curves for neutral atoms taken from the International Tables for Crystallography.[39] The site occupancy factors (s.o.f.) are given in Supporting Information Table ST3. At this point, taking into account: (i) the observed bond distances (Supporting Information Table ST4), (ii) the bond valence sums, and (iii) the s.o.f. occurring at the M sites (Supporting Information Table ST5), we proposed the following site populations: $M1$ = $Mg_{0.45}Si_{0.40}Fe_{0.15}$; $M2$ = $Mg_{0.43}Si_{0.34}Fe_{0.23}$; $M3$ = $Mg_{0.55}Si_{0.36}Fe_{0.09}$; and $M4$ = $Mg_{0.50}Fe_{0.40}Si_{0.10}$. Such populations were then fixed at the M sites in the subsequent refinement cycles. We attempted to refine an anisotropic model of the structure, but several ADPs were nonpositive definite. For these reasons, here, we present an isotropic model of the structure. R = 0.0309 for 230 reflections with $F_o > 4\sigma(F_o)$. Crystallographic data (CCDC 2050890) can be obtained free of charge from the Cambridge Crystallographic Data Centre via www.ccdc.cam.ac.uk/data_request/cif.

The crystal structure of the elgoresyite grain is shown in Figure 2. It is isostructural with the high-pressure iron oxide

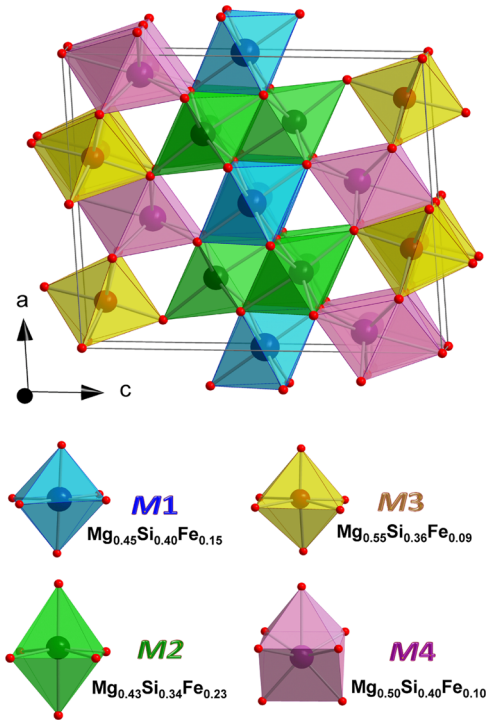

Figure 2. Crystal structure of elgoresyite. Large circles are atomic positions for Mg, Si, and Fe. Red small circles indicate oxygen atoms. MO_6 polyhedra for $M1$, $M2$, $M3$, and $M4$ sites are shown by transparent blocks with different colors. The unit cell and the orientation of the structure are outlined.

Fe_7O_9[22] (Figure 2) with four different crystallographic sites for cations. Three are octahedrally coordinated and connected in a 3D network ($M1$, $M2$, and $M3$), while the fourth, $M4$, has a trigonal-prismatic geometry with an additional long bond with O2 (Supporting Information Table ST4). As already pointed out by Sinmyo et al.,[22] $M4$ is the bigger site and hosts the largest cations (i.e., Fe^{2+} and probably also the minor amounts of Na and Ca). The unit cell parameters of the new phase are influenced by the incorporation of Si into the structure. We observed a general reduction of the unit cell from pure [a = 9.696(2) Å, b = 2.8947(6) Å, c = 11.428(3) Å, β = 101.69(2)°, and V = 314.10(12) Å^3] to Mg-doped Fe_7O_9 [a = 9.6901(12) Å, b = 2.8943(5) Å, c = 11.4397(15) Å, β = 102.045(14)°, and V = 313.77(8) Å^3].[22] The assignment of Si substituting for Mg/Fe at the M sites is required both to account for the electron density at that site and to justify the decrease of the mean bond distances relative to pure and Mg-doped Fe_7O_9.[22] The Mg/Fe-for-Si substitution has different effects on the distortion of the M sites. In particular, we observed an increase in the bond-angle variance σ^2[40] of the $M1$ site from 9.69 in Mg-doped Fe_7O_9,[22] through 11.38 in pure Fe_7O_9[22] to 25.30 in the new phase. In contrast, we observed a decrease in σ^2 of the $M2$ site from 76.79 in pure Fe_7O_9 through 66.57 in Mg-doped Fe_7O_9 to 56.56 in the new phase.[22] The values of the σ^2 bond-angle variance for $M3$ and $M4$ are similar in the three structures.

https://doi.org/10.1021/acsearthspacechem.1c00157
ACS Earth Space Chem. 2021, 5, 2124–2130

DISCUSSION

The striking similarity of crystal structures of Fe_7O_9[22] and $(Mg,Fe)_5Si_2O_9$ can be explained by the $M^{2+} + Si^{4+} = 2Fe^{3+}$ coupled substitution. The ionic radii of the sixfold coordinated cations are 0.72 and 0.40 Å for Mg^{2+} and Si^{4+}, respectively, and their mean value of 0.56 Å is comparable with 0.645 (high-spin) or 0.55 Å (low-spin) of Fe^{3+}.[41] Mg^{2+}, Fe^{2+}, and Si^{4+} occupy $M1-M4$ sites of the $(Mg,Fe)_5Si_2O_9$ structure in a less ordered manner compared to Si-free Fe_7O_9. This is likely because the crystal structure of $(Mg,Fe)_5Si_2O_9$ is based solely on octahedra with similar size (Figure 2). In contrast, known high-pressure polymorphs of magnesium silicates contain distinguishable sites for Si^{4+} and M^{2+}. For example, the respective coordination numbers are 4 and 6 for SiO_4 and MO_6 in ringwoodite and 6 and 8 for SiO_6 and MO_8 in bridgmanite. Cations in the newly found iron-magnesium silicate (elgoresyite) are in coordination geometries of $SiO_6 + MO_6$, which are in between $SiO_4 + MO_6$ for ringwoodite and $SiO_6 + MgO_8$ for bridgmanite. This suggests that $(Mg,Fe)_5Si_2O_9$ is an intermediate phase at pressures characteristic for the existence of ringwoodite and bridgmanite. Nevertheless, since the stability is not well known yet, we cannot rule out the possibility that $(Mg,Fe)_5Si_2O_9$ is a metastable phase. It should be studied further by experiments and theory.

By analogy with the $(FeO)_m(Fe_2O_3)_n$ series, magnesium silicates may also form homologous series with a chemistry of $(MgO)_{m+n}(SiO_2)_n$ or $Mg_{m+n}Si_nO_{m+3n}$ via the $Mg^{2+} + Si^{4+} = 2Fe^{3+}$ substitution (Figure 3). We can easily propose solid solutions like Fe_4O_5-Mg_3SiO_5, Fe_5O_6-Mg_4SiO_6, Fe_9O_{11}-$Mg_7Si_2O_{11}$, Fe_5O_7-$Mg_3Si_2O_7$, and so on. Indeed, it was shown that a high-pressure polymorph of Fe_2O_3 (ζ-phase) exhibits a perovskite-type crystal structure very similar to that of $MgSiO_3$ bridgmanite.[23] This is likely a result of $Mg^{2+} + Si^{4+} = 2Fe^{3+}$ substitution in Fe_2O_3-$MgSiO_3$ at high pressure.

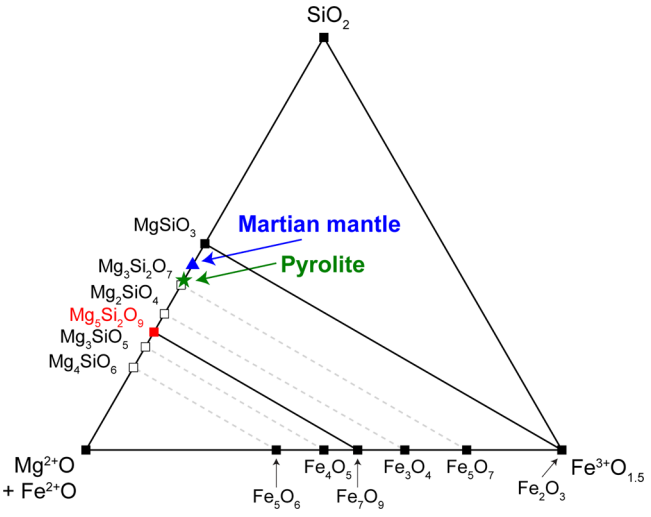

Figure 3. High-pressure phase diagram of Mg-Fe-Si oxides. Tentative subsolidus phase diagram in the $(Mg^{2+} + Fe^{2+})O$-SiO_2-$Fe^{3+}O_{1.5}$ ternary system showing potential homologous series of $(FeO)_m(Fe_2O_3)_n$-$(MgO)_{m+n}(SiO_2)_n$. Filled symbols are already confirmed phases including $Mg_5Si_2O_9$ by this study (red). Open symbols are possible magnesium silicate series with the chemistry of $(MgO)_{m+n}(SiO_2)_n$. Lines are tie lines for the phases with the same crystal structure. Solid lines are already confirmed pairs, and broken lines are not reported yet. The green star and blue triangle correspond to pyrolite and Martian mantle composition, respectively.

Bridgmanite and Fe_2O_3 (ζ-phase) are stable above 24 and 50 GPa, respectively. Moreover, Fe_2O_3 with the $CaIrO_3$-type crystal structure (η-phase) and $MgSiO_3$ post-perovskite also possess the same structural type (orthorhombic space group $Cmcm$).[3,23,42] Post-perovskite magnesium silicate and Fe_2O_3 (η-phase) are stable above 120 and 60 GPa, respectively. Mg-sites in bridgmanite and the post-perovskite phase correspond to the $Fe^{3+}O_6$ trigonal prism sites in the crystal structure of ζ- and η-Fe_2O_3.[23] Small tilts and distortions of polyhedra in the high-pressure homologous iron oxides may lead to an increase in the coordination number from FeO_6 trigonal prism sites to MO_8 sites in iron-magnesium silicates. Indeed, the distortion factor is significantly larger in $(Mg,Fe)_5Si_2O_9$ compared to Fe_7O_9 (see Methods and Results). It is reported that $NaMnF_3$, an analog of $MgSiO_3$ perovskite, decomposes into $Na_3Mn_2F_7 + MnF_2$ at 10 GPa and 1273 K instead of undergoing a phase transition to post-perovskite,[43] while the crystal structure of $Na_3Mn_2F_7$ has not yet been determined. This suggests that $Mg_3Si_2O_7$ may be stable at certain high-pressure and high-temperature conditions. Mg_3SiO_5 with the Cm space group was reported to be unstable at high pressure based on theoretical calculations to seek candidates for post-post-perovskite phase transitions.[44] Instead, Mg_3SiO_5 is possibly stable with a similar crystal structure to Fe_4O_5 with the $Cmcm$ space group.[19] Previous studies reported that the Fe_5O_6 phase was coexisting with silicate phases (ringwoodite or wadsleyite) without containing any silicon up to 1873 K.[45,46] However, the experimental temperature was significantly lower than the liquidus temperature at which likely $(Mg, Fe)_5Si_2O_9$ was formed. As a foundation for further discussion, it is required to study the stability of the phases at higher temperature conditions in systems such as Fe_4O_5-Mg_3SiO_5, Fe_5O_6-Mg_4SiO_6, Fe_7O_9-$Mg_5Si_2O_9$, and so on.

Since $Mg_5Si_2O_9$ is more enriched in MgO than Mg_2SiO_4, new magnesium silicate is unlikely to play a significant role in the bulk part of Earth's mantle, whose chemistry is between Mg_2SiO_4 and $MgSiO_3$. Nevertheless, elgoresyite could play an important role in the dynamics of rocky planetary interiors with higher (Mg,Fe)O content than Earth's mantle.

The observed shock-induced melt vein likely experienced high-pressure conditions around ~23 GPa since it contains ringwoodite. Assuming that the surrounding silicate glass was derived from melt, temperatures may have exceeded ~2000 K according to the eutectic melting temperature.[9] Coexisting $MgSiO_3$-rich glass suggests that the new phase is potentially a liquidus phase of silicate melt at high pressure. Mg_2SiO_4 in the host rock could have been incongruently melted to form the $MgSiO_3$-rich melt and the new iron-magnesium silicate during shock events. The presence of only Fe^{2+} in the new magnesium silicate may be partly a consequence of melting, since Fe^{3+} is more incompatible.[47] Accordingly, elgoresyite could be first crystallized from deep magmas, such as in a magma ocean, redox-induced melt, or dehydration-induced melt.[47−50] The magma ocean would be enriched in (MgO + FeO) relative to chondrite at later stages of freezing because of the crystallization of bridgmanite-rich material.[9] Elgoresyite could therefore be crystallized from a magma ocean at a specific depth and time. The newly discovered phase and the possible homologous series of magnesium silicates could significantly affect chemical evolution of the magma ocean, since the density of the liquidus phase controls the fate of crystallized solids during freezing of the magma ocean.[10,48]

https://doi.org/10.1021/acsearthspacechem.1c00157
ACS Earth Space Chem. 2021, 5, 2124−2130

Redox-induced melting of carbonaceous material may generate a melt deeper than 250 km.[49] While phase relationships are more complicated in the carbon-bearing system, carbonaceous magma is relatively enriched in (MgO + FeO)/SiO_2,[49] and accordingly, elgoresyite may be captured by a diamond ascending by upwelling carbonaceous magma in the mantle. Indeed, the pair MgO + Mg_2SiO_4 was found in diamond inclusions from Kankan, Juina, and Panda.[17] It may represent relics of the new magnesium silicate $Mg_5Si_2O_9$.

Although the chemistry of the Martian mantle is still unclear,[51] it is interesting to speculate on the possible presence of elgoresyite in the red planet. On the one hand, the Mars mantle has been estimated to contain more (MgO + FeO) compared to Earth,[52] has lower pressures and temperatures, and thus elgoresyite, $(Mg,Fe)_5Si_2O_9$, might be present. On the other hand, according to ref 53 and the references therein, the weight fraction of FeO in the Martian mantle is higher than that in Earth's mantle peridotite, while the (Mg + Fe)/Si molar ratio is 1.35[54] rather lower than that in Earth's mantle peridotite[55] and pyrolite[56] (Figure 3), indicating that the formation of elgoresyite in the Martian mantle is unlikely.

While phase relationships of magnesium silicates have been repeatedly studied by experiments around liquidus temperatures, phases are usually determined by chemical analysis using an electron microscope and an electron microprobe. Since chemical compositions of the new iron-magnesium silicate are similar to ringwoodite, liquidus phases can be easily misidentified. The stability of magnesium silicates should be studied using methods that provide finer detail.

■ ASSOCIATED CONTENT

Supporting Information

The Supporting Information is available free of charge at https://pubs.acs.org/doi/10.1021/acsearthspacechem.1c00157.

Analytical data (in wt %) for the new magnesium silicate; X-ray powder diffraction data (d in Å) for the new magnesium silicate; atoms, Wyckoff positions, mean electron numbers, proposed site populations, fractional coordinates of atoms, and isotropic displacement parameters in the structure of the new magnesium silicate; selected bond distances (Å) in the structure of the new magnesium silicate; and bond valence sums calculated with the site populations (Tables ST1−ST5) (PDF)

■ AUTHOR INFORMATION

Corresponding Author

Luca Bindi − *Dipartimento di Scienze della Terra, Università degli Studi di Firenze, Firenze I-50121, Italy;* orcid.org/0000-0003-1168-7306; Email: luca.bindi@unifi.it

Authors

Ryosuke Sinmyo − *Department of Physics, School of Science and Technology, Meiji University, Kanagawa 101-8301, Japan*

Elena Bykova − *Bayerisches Geoinstitut, Universität Bayreuth, Bayreuth D-95440, Germany; Laboratory of Crystallography, Universität Bayreuth, Bayreuth D-95447, Germany*

Sergey V. Ovsyannikov − *Bayerisches Geoinstitut, Universität Bayreuth, Bayreuth D-95440, Germany; Institute for Solid State Chemistry of Ural Branch of Russian Academy of Sciences, Yekaterinburg 620219, Russia;* orcid.org/0000-0003-1027-0998

Catherine McCammon − *Bayerisches Geoinstitut, Universität Bayreuth, Bayreuth D-95440, Germany*

Ilya Kupenko − *European Synchrotron Radiation Facility, Grenoble F-38043, France*

Leyla Ismailova − *Bayerisches Geoinstitut, Universität Bayreuth, Bayreuth D-95440, Germany; Laboratory of Crystallography, Universität Bayreuth, Bayreuth D-95447, Germany*

Leonid Dubrovinsky − *Bayerisches Geoinstitut, Universität Bayreuth, Bayreuth D-95440, Germany*

Xiande Xie − *Key Laboratory of Mineralogy and Metallogeny, Guangzhou Institute of Geochemistry, Chinese Academy of Sciences, Guangzhou 510640, China; Guangdong Provincial Key Laboratory of Mineral Physics and Materials, Guangzhou 510640, China*

Complete contact information is available at: https://pubs.acs.org/10.1021/acsearthspacechem.1c00157

Notes

The authors declare no competing financial interest.

Additional information about the new silicate is provided as Supporting information. Crystallographic data (CCDC 2050890) can be obtained free of charge from the Cambridge Crystallographic Data Centre via www.ccdc.cam.ac.uk/data_request/cif. The main data are contained in the paper. All other relevant data are available from the corresponding author upon request.

■ ACKNOWLEDGMENTS

We acknowledge Teresa Salvatici for the preparation of the studied sample. L.B. is funded by MIUR-PRIN2017, project "TEOREM − deciphering geological processes using Terrestrial and Extraterrestrial ORE Minerals", prot. 2017AK8C32 (PI: Luca Bindi); S.V.O. acknowledges the financial support from the Deutsche Forschungsgemeinschaft (DFG, Grant. No. OV-110/3-2).

■ REFERENCES

(1) Liu, L.-G. Silicate perovskite from phase transformations of pyrope-garnet at high pressure and temperature. *Geophys. Res. Lett.* **1974**, *1*, 277−280.

(2) Ito, E. The absence of oxide mixture in high-pressure phases of Mg-silicates. *Geophys. Res. Lett.* **1977**, *4*, 72−74.

(3) Murakami, M.; Hirose, K.; Kawamura, K.; Sata, N.; Ohishi, Y. Post-perovskite phase transition in $MgSiO_3$. *Science* **2004**, *304*, 855−858.

(4) Ringwood, A. E.; Major, A. The system Mg_2SiO_4-Fe_2SiO_4 at high pressures and temperatures. *Phys. Earth Planet. Inter.* **1970**, *3*, 89−108.

(5) Tackley, P. J.; Stevenson, D. J.; Glatzmaier, G. A.; Schubert, G. Effects of an endothermic phase transition at 670 km depth in a spherical model of convection in the Earth's mantle. *Nature* **1993**, *361*, 699−704.

(6) Matyska, C.; Yuen, D. The importance of radiative heat transfer on superplumes in the lower mantle with the new post-perovskite phase change. *Earth Planet. Sci. Lett.* **2005**, *234*, 71−81.

(7) Tschauner, O.; Ma, C.; Beckett, J. R.; Prescher, C.; Prakapenka, V. B.; Rossman, G. R. Discovery of bridgmanite, the most abundant mineral in Earth, in a shocked meteorite. *Science* **2014**, *346*, 1100−1102.

(8) Breuer, D.; Yuen, D. A.; Spohn, T.; Zhang, S. Three dimensional models of Martian mantle convection with phase transitions. *Geophys. Res. Lett.* **1998**, *25*, 229−232.
(9) Boukaré, C. E.; Ricard, Y.; Fiquet, G. Thermodynamics of the MgO-FeO-SiO_2 system up to 140 GPa: Application to the crystallization of Earth's magma ocean. *J. Geophys. Res.-Solid Earth* **2015**, *120*, 6085−6101.
(10) Ohtani, E. The primordial terrestrial magma ocean and its implication for stratification of the mantle. *Phys. Earth Planet. Inter.* **1985**, *38*, 70−80.
(11) Ozawa, K.; Anzai, M.; Hirose, K.; Sinmyo, R.; Tateno, S. Experimental Determination of Eutectic Liquid Compositions in the MgO-SiO_2 System to the Lowermost Mantle Pressures. *Geophys. Res. Lett.* **2018**, *45*, 9552−9558.
(12) Ballmer, M. D.; Houser, C.; Hernlund, J. W.; Wentzcovitch, R. M.; Hirose, K. Persistence of strong silica-enriched domains in the Earth's lower mantle. *Nat. Geosci.* **2017**, *10*, 236−240.
(13) Collerson, K. D.; Hapugoda, S.; Kamber, B. S.; Williams, Q. Rocks from the mantle transition zone: Majorite-bearing xenoliths from Malaita, Southwest Pacific. *Science* **2000**, *288*, 1215−1223.
(14) Pearson, D. G.; Brenker, F. E.; Nestola, F.; McNeill, J.; Nasdala, L.; Hutchison, M. T.; Matveev, S.; Mather, K.; Silversmit, G.; Schmitz, S.; Vekemans, B.; Vincze, L. Hydrous mantle transition zone indicated by ringwoodite included within diamond. *Nature* **2014**, *507*, 221−224.
(15) Binns, R. A.; Davis, R. J.; Reed, S. J. B. Ringwoodite, natural $(Mg,Fe)_2SiO_4$ spinel in the Tenham meteorite. *Nature* **1969**, *221*, 943−944.
(16) Bindi, L.; Shim, S.-H.; Sharp, T. G.; Xie, X. Evidence for the charge disproportionation of iron in extraterrestrial bridgmanite. *Sci. Adv.* **2020**, *6*, No. eaay7893.
(17) Harte, B. Diamond formation in the deep mantle: the record of mineral inclusions and their distribution in relation to mantle dehydration zones. *Mineral. Mag.* **2010**, *74*, 189−215.
(18) Walter, M. J.; Kohn, S. C.; Araujo, D.; Bulanova, G. P.; Smith, C. B.; Gaillou, E.; Wang, J.; Steele, A.; Shirey, S. B. Deep mantle cycling of oceanic crust: evidence from diamonds and their mineral inclusions. *Science* **2011**, *334*, 54−57.
(19) Lavina, B.; Dera, P.; Kim, E.; Meng, Y.; Downs, R. T.; Weck, P. F.; Sutton, S. R.; Zhao, Y. Discovery of the recoverable high-pressure iron oxide Fe_4O_5. *Proc. Natl. Acad. Sci. U. S. A.* **2011**, *108*, 17281−17285.
(20) Lavina, B.; Meng, Y. Unraveling the complexity of iron oxides at high pressure and temperature: Synthesis of Fe_5O_6. *Sci. Adv.* **2015**, *1*, No. e1400260.
(21) Ishii, T.; Uenver-Thiele, L.; Woodland, A. B.; Alig, E.; Ballaran, T. B. Synthesis and crystal structure of Mg-bearing Fe_9O_{11}: New insight in the complexity of Fe-Mg oxides at conditions of the deep upper mantle. *Am. Mineral.* **2018**, *103*, 1873−1876.
(22) Sinmyo, R.; Bykova, E.; Ovsyannikov, S. V.; McCammon, C.; Kupenko, I.; Ismailova, L.; Dubrovinsky, L. Discovery of Fe_7O_9: a new iron oxide with a complex monoclinic structure. *Sci. Rep.* **2016**, *6*, 32852.
(23) Bykova, E.; Dubrovinsky, L.; Dubrovinskaia, N.; Bykov, M.; McCammon, C.; Ovsyannikov, S. V.; Liermann, H. P.; Kupenko, I.; Chumakov, A. I.; Rüffer, R.; Hanfland, M.; Prakapenka, V. Structural complexity of simple Fe_2O_3 at high pressures and temperatures. *Nat. Commun.* **2016**, *7*, 10661.
(24) Anzolini, C.; Marquardt, K.; Stagno, V.; Bindi, L.; Frost, D. J.; Pearson, D. G.; Harris, J. W.; Hemley, R. J.; Nestola, F. Evidence for complex iron oxides in the deep mantle from FeNi (Cu) inclusions in superdeep diamond. *Proc. Natl. Acad. Sci.* **2020**, *117*, 21088−21094.
(25) Jacob, D. E.; Piazolo, S.; Schreiber, A.; Trimby, P. Redox-freezing and nucleation of diamond via magnetite formation in the Earth's mantle. *Nat. Commun.* **2016**, *7*, 11891.
(26) Bindi, L.; Brenker, F. E.; Nestola, F.; Koch, T. E.; Prior, D. J.; Lilly, K.; Krot, A. N.; Bizzarro, M.; Xie, X. Discovery of asimowite, the Fe-analog of wadsleyite, in shock-melted silicate droplets of the Suizhou L6 and the Quebrada Chimborazo 001 CB3. 0 chondrites. *Am. Mineral.* **2019**, *104*, 775−778.
(27) Bindi, L.; Chen, M.; Xie, X. Discovery of the Fe-analogue of akimotoite in the shocked Suizhou L6 chondrite. *Sci. Rep.* **2017**, *7*, 42674.
(28) Chen, M.; Shu, J.; Mao, H.-K. Xieite, a new mineral of high-pressure $FeCr_2O_4$ polymorph. *Chin. Sci. Bull.* **2008**, *53*, 3341−3345.
(29) Chen, M.; Shu, J.; Mao, H.-k.; Xie, X.; Hemley, R. J. Natural occurrence and synthesis of two new postspinel polymorphs of chromite. *Proc. Natl. Acad. Sci.* **2003**, *100*, 14651−14654.
(30) Chen, M.; Shu, J.; Xie, X.; Mao, H.-k. Natural $CaTi_2O_4$-structured $FeCr_2O_4$ polymorph in the Suizhou meteorite and its significance in mantle mineralogy. *Geochim. Cosmochim. Acta* **2003**, *67*, 3937−3942.
(31) Chen, M.; Xie, X. Shock-produced akimotoite in the Suizhou L6 chondrite. *Sci. China Earth Sci.* **2015**, *58*, 876−880.
(32) Chen, M.; Xie, X.; Goresy, A. E. L. A shock-produced (Mg, Fe) SiO_3 glass in the Suizhou meteorite. *Meteorit. Planet. Sci.* **2004**, *39*, 1797−1808.
(33) Ma, C.; Tschauner, O.; Bindi, L.; Beckett, J. R.; Xie, X. A vacancy-rich, partially inverted spinelloid silicate,$(Mg, Fe, Si)_2(Si,\square)$-$O_4$, as a major matrix phase in shock melt veins of the Tenham and Suizhou L6 chondrites. *Meteorit. Planet. Sci.* **2019**, *54*, 1907−1918.
(34) Xie, X.; Chen, M.; Wang, D. Shock-related mineralogical features and PT history of the Suizhou L6 chondrite. *Eur. J. Mineral.* **2001**, *13*, 1177−1190.
(35) Xie, X.; Minitti, M. E.; Chen, M.; Mao, H.-K.; Wang, D.; Shu, J.; Fei, Y. Tuite, γ-$Ca_3(PO_4)_2$: A new mineral from the Suizhou L6 chondrite. *Eur. J. Mineral.* **2004**, *15*, 1001−1005.
(36) Xie, X.; Sun, Z.; Chen, M. The distinct morphological and petrological features of shock melt veins in the Suizhou L6 chondrite. *Meteorit. Planet. Sci.* **2011**, *46*, 459−469.
(37) Bruker, A. APEX3 Package, APEX3, SAINT and SADABS. 2016.
(38) Sheldrick, G. M. A short history of SHELX. *Acta Crystallogr., Sect. A: Found. Crystallogr.* **2008**, *64*, 112−122.
(39) Wilson, A. J. C.; Geist, V. International Tables for Crystallography. Volume C: Mathematical, Physical and Chemical Tables. Kluwer Academic Publishers, Dordrecht/Boston/London 1992 (published for the International Union of Crystallography), 883 Seiten, ISBN 0-792-3-16-38X. *Cryst. Res. Technol.* **1993**, *28*, 110−110.
(40) Robinson, K.; Gibbs, G. V.; Ribbe, P. H. Quadratic elongation: a quantitative measure of distortion in coordination polyhedra. *Science* **1971**, *172*, 567−570.
(41) Shannon, R. D. Revised effective ionic radii and systematic studies of interatomic distances in halides and chalcogenides. *Acta Cryst. A* **1976**, *32*, 751−767.
(42) Ono, S.; Kikegawa, T.; Ohishi, Y. High-pressure phase transition of hematite, Fe_2O_3. *J. Phys. Chem. Solids* **2004**, *65*, 1527−1530.
(43) Akaogi, M.; Shirako, Y.; Kojitani, H.; Nagakari, T.; Yusa, H.; Yamaura, K. High-pressure transitions in $NaZnF_3$ and $NaMnF_3$ perovskites, and crystal-chemical characteristics of perovskite-postperovskite transitions in ABX_3 fluorides and oxides. *Phys. Earth Planet. Inter.* **2014**, *228*, 160−169.
(44) Umemoto, K.; Wentzcovitch, R. M.; Wu, S. Q.; Ji, M.; Wang, C. Z.; Ho, K. M. Phase transitions in $MgSiO_3$ post-perovskite in super-Earth mantles. *Earth Planet. Sci. Lett.* **2017**, *478*, 40−45.
(45) Uenver-Thiele, L.; Woodland, A. B.; Miyajima, N.; Ballaran, T. B.; Frost, D. J. Behaviour of Fe_4O_5−$Mg_2Fe_2O_5$ solid solutions and their relation to coexisting Mg−Fe silicates and oxide phases. *Contrib. Mineral. Petrol.* **2018**, *173*, 20.
(46) Woodland, A. B.; Schollenbruch, K.; Koch, M.; Ballaran, T. B.; Angel, R. J.; Frost, D. J. Fe_4O_5 and its solid solutions in several simple systems. *Contrib. Mineral. Petrol.* **2013**, *166*, 1677−1686.
(47) Sinmyo, R.; Nakajima, Y.; McCammon, C. A.; Miyajima, N.; Petitgirard, S.; Myhill, R.; Dubrovinsky, L.; Frost, D. J. Effect of Fe^{3+} on phase relations in the lower mantle: Implications for redox melting

in stagnant slabs. *J. Geophys. Res.: Solid Earth* **2019**, *124*, 12484−12497.
(48) Labrosse, S.; Hernlund, J. W.; Coltice, N. A crystallizing dense magma ocean at the base of the Earth's mantle. *Nature* **2007**, *450*, 866−869.
(49) Rohrbach, A.; Schmidt, M. W. Redox freezing and melting in the Earth's deep mantle resulting from carbon−iron redox coupling. *Nature* **2011**, *472*, 209−212.
(50) Schmandt, B.; Jacobsen, S. D.; Becker, T. W.; Liu, Z. X.; Dueker, K. G. Dehydration melting at the top of the lower mantle. *Science* **2014**, *344*, 1265−1268.
(51) Yoshizaki, T.; McDonough, W. F. The composition of Mars. *Geochim. Cosmochim. Acta* **2020**, *273*, 137−162.
(52) Wänke, H.; Dreibus, G. Chemical composition and accretion history of terrestrial planets. *Phil. Trans. R. Soc. Lond. A* **1988**, *325*, 545−557.
(53) Bertka, C. M.; Fei, Y. Mineralogy of the Martian interior up to core-mantle boundary pressures. *J. Geophys. Res.* **1997**, *102*, 5251−5264.
(54) Dreibus, G.; Wänke, H. Mars, a volatile-rich plant. *Meteoritics* **1985**, *20*, 367−381.
(55) Takahashi, E. Melting of a dry peridotite KLB-1 up to 14 GPa: Implications on the Origin of peridotitic upper mantle. *J. Geophys. Res.* **1986**, *91*, 9367−9382.
(56) Irifune, T. Phase transformations in the earth's mantle and subducting slabs: Implications for their compositions, seismic velocity and density structures and dynamics. *Island Arc* **1993**, *2*, 55−71.

https://doi.org/10.1021/acsearthspacechem.1c00157
ACS Earth Space Chem. 2021, 5, 2124−2130